# Theoretical models of Rashba spin splitting in asymmetric $SrTiO_3$-based heterostructures

L. W. van Heeringen,[1] A. McCollam,[1,2] G. A. de Wijs,[1] and A. Fasolino[1]

[1]*Institute for Molecules and Materials, Radboud University, Heyendaalseweg 135, 6525 AJ Nijmegen, The Netherlands*

[2]*High Field Magnet Laboratory (HFML-EMFL), Radboud University, 6535 ED Nijmegen, The Netherlands*

(Received 24 October 2016; revised manuscript received 21 February 2017; published 19 April 2017)

Rashba spin splitting in two-dimensional (2D) semiconductor systems is generally calculated in a $\mathbf{k}\cdot\mathbf{p}$ Luttinger-Kohn approach where the spin splitting due to asymmetry emerges naturally from the bulk band structure. In recent years, several new classes of 2D systems have been discovered where electronic correlations are believed to have an important role. In these correlated systems, the effects of asymmetry leading to Rashba splitting have typically been treated phenomenologically. We compare these two approaches for the case of 2D electron systems in $SrTiO_3$-based heterostructures, and find that the two models produce fundamentally different behavior in regions of the Brillouin zone that are particularly relevant for magnetotransport. Our results demonstrate the importance of identifying the correct approach in the quantitative interpretation of experimental data, and are likely to be relevant to a range of 2D systems in correlated materials.

DOI: 10.1103/PhysRevB.95.155134

## I. INTRODUCTION

The discovery of a two-dimensional (2D) electron system at the $LaAlO_3/SrTiO_3$ (LAO/STO) interface [1] has generated a large interest in this topic, due to the realization of a new class of materials based on transition metal oxide heterostructures, and also to the diverse phenomena that they exhibit, such as superconductivity, magnetism, and strong spin-orbit interactions, all of which can be tuned by an external electric field [2–7]. The development of heterostructures made from materials traditionally studied for correlated electron effects such as high-temperature superconductivity, Mott physics, and quantum magnetism, invites us to inquire whether approaches that have been successful for semiconductor heterostructures can become relevant for this new class of materials [8]. A key connection to semiconductor physics comes through STO, where strong spin-orbit coupling deeply affects the free-electron character of the bulk electronic bands, such that they can be theoretically described in ways analogous to the hole bands in III-V semiconductors [9] (see Fig. 1). Recently, many experimental results have addressed the Rashba spin splitting due to asymmetry at the interfaces in oxide heterostructures in the presence of spin-orbit coupling [4,10–16]. It is also important to consider the effect of unintentional asymmetry in nominally symmetric systems, such as $\delta$-doped materials [17]. Here, we compare the effect on a given conduction band structure of two descriptions of the Rashba spin splitting that have been developed independently in the two fields of semiconductors and correlated electrons. Our results show a clear difference between the two descriptions that could be important for the interpretation of experimental results, in particular, as a consequence of the different resulting Fermi surfaces. Our findings will also have relevance to other 2D systems in correlated materials where spin-orbit coupling and Rashba effects are important, such as topological insulators, iridium oxides, and skyrmionic systems [6,18–21].

In the field of correlated electrons, it has become customary to assume that a suitable description of the spin splitting due to asymmetry can be obtained by adding to the Hamiltonian the following phenomenological term [15,22–26],

$$H^{\gamma} = \gamma \begin{pmatrix} 0 & 0 & 2i\sin(k_x) \\ 0 & 0 & 2i\sin(k_y) \\ -2i\sin(k_x) & -2i\sin(k_y) & 0 \end{pmatrix}. \quad (1)$$

This model depends on the scalar parameter $\gamma$, which is a measure of the asymmetry of atomic orbitals at the interface.

Alternatively, within the $\mathbf{k}\cdot\mathbf{p}$ Luttinger-Kohn (LK) method [27] of spin-orbit coupled bulk bands, the spin splitting follows naturally from the nonsymmetric confining potential. This approach is well established for semiconductors [9,28–32] and has been shown to produce Rashba spin splittings in the $LaAlO_3/SrTiO_3$ heterostructure in Ref. [33]. Although both models, hereafter referred to as the $\gamma$ model and the LK model, aim to capture the asymmetry of the system, the resulting spin splittings are in fact qualitatively and quantitatively different due to fundamental differences in the underlying Hamiltonians that we describe in the following. These differences can be crucial in the interpretation of magnetotransport measurements that measure the effect of Rashba spin splitting to extract details of the band structure [4,10–16].

It is still an open question which asymmetry is dominant in $SrTiO_3$-based heterostructures, a localized distortion of atomic orbitals at the interface or an effective asymmetric confining potential acting on more extended wave functions in $SrTiO_3$ [22,33,34]. Measurements of the Rashba spin splitting can help to answer this question, but the issue is complicated by the fact that access to the Rashba spin splittings is usually indirect, via either weak antilocalization or Shubnikov–de Haas (SdH) oscillations.

To make a correct identification attainable, we compare the Rashba spin splittings as produced by the $\gamma$ and the LK models and identify the key differences. We find that the two models give comparable spin splitting of the lowest heavy electron states if the parameter $\gamma$ is suitably chosen. At higher energies, in the vicinity of typical Fermi energies, the $\gamma$ model gives

 

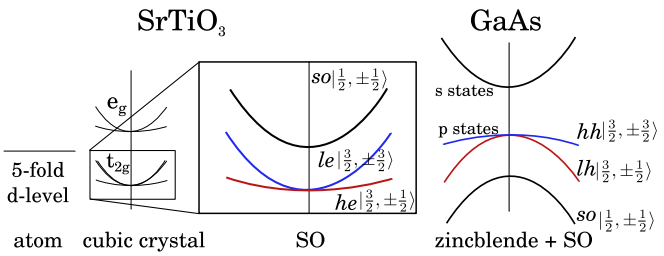


FIG. 1. Comparison of the conduction band $d$ states in $SrTiO_3$ with the hole band $p$ states in GaAs (see text). The color red (blue) indicates $m_j = \pm\frac{3}{2}$ ($m_j = \pm\frac{1}{2}$) bands to point out the reversal of the heavy and light mass.

much larger spin splittings than the LK model, with a different wave-vector dependence. These differences lead to different Fermi surfaces in the two models. This means that it would be possible to discriminate between them by SdH experiments [35] if the Fermi energy is swept, e.g., by gating, through the energy range of the subband anticrossing and beyond, where the models differ significantly.

In Sec. II we describe the orbital character of the relevant electrons and compare them to the hole states in III-V semiconductors where the LK model is routinely used for calculations of the electronic structure. In Sec. III we discuss the origin of the Rashba splitting for spin-orbit (SO) coupled bands in asymmetric potentials. In Sec. IV we show how the bulk bands are changed by SO coupling within the LK formalism. In particular, we discuss how the $d_{xy}$, $d_{yz}$, and $d_{xz}$ states transform in the presence of SO coupling to the light electrons ($le$), heavy electrons ($he$), and split-off ($so$) bands. We also introduce the LK coupling Hamiltonian $H^{\mathrm{LK}}_{\uparrow\downarrow}$. In Sec. V, we introduce the $H^{\gamma}_{\uparrow\downarrow}$ for the $\gamma$ model and we compare it to $H^{\mathrm{LK}}_{\uparrow\downarrow}$ in Sec. VI. Section VII is devoted to a comparison of the results of the two models for the Rashba spin splitting. Conclusions and perspectives are given in Sec. VIII.

## II. CHARACTER OF SO-COUPLED BANDS

The conduction band edge of $SrTiO_3$ has strong similarities to the valence band of III-V semiconductors, and formally the same Luttinger-Kohn (LK) Hamiltonian [Eq. (4)] can be used to describe quantitatively the conduction electrons. In the III-V semiconductors, this Hamiltonian, combined with the envelope function method, has been very successful in the study of heterostructures [9]. That a material where the conduction band consists of $d$-level states turns out to be similar to that of $p$-level valence states in III-V semiconductors may seem surprising. In Fig. 1 we sketch the relation between the conduction band in $SrTiO_3$ and the valence band in III-V semiconductors. In $SrTiO_3$ the cubic crystal field splits the fivefold degenerate atomic $d$ levels (tenfold counting spin) into the threefold degenerate $t_{2g}$ states ($d_{xy}$, $d_{yz}$, and $d_{zx}$) and the twofold degenerate $e_g$ states. At $\Gamma$, the symmetry of the $t_{2g}$ states is $\Gamma^+_{25}$, the same as for the $p$ states in the zinc-blende structure of III-V semiconductors [36,37]. SO coupling lifts the degeneracy further into a heavy and light electron band ($he$,$le$) corresponding to a total angular momentum $J = \frac{3}{2}$ and a split-off band ($so$) with $J = \frac{1}{2}$, analogous to the heavy and light holes ($hh$,$lh$) and split-off holes ($so$) in III-V semiconductors. A noticeable difference is that the nature of the basis set ($d$ or $p$) makes that the orbital character of the *light* electrons corresponds to the *heavy* holes and vice versa, as indicated by the colors in Fig. 1. We emphasize that due to strong SO coupling in $SrTiO_3$, labeling electrons as $d_{xy}$ or $d_{yz}$ states is not correct, and classification in terms of the total angular momentum $J$ is necessary.

## III. RASHBA SPIN SPLITTING

In bulk systems and symmetric heterostructures, bands are spin degenerate (in the absence of a magnetic field). In fact, space inversion symmetry $E(k,\uparrow) = E(-k,\uparrow)$ combined with time reversal symmetry (Kramers degeneracy) $E(k,\uparrow) = E(-k,\downarrow)$ yields $E(-k,\uparrow) = E(-k,\downarrow)$. If space reversal symmetry is broken, bands can spin split, although they still obey Kramers degeneracy. When such a spin splitting is a result of an asymmetric confining potential, it is called Rashba spin splitting, named after Rashba, who first described it for a simple two-band model [38]. Today, the term Rashba spin splitting is also used to describe multiband systems such as $SrTiO_3$-based heterostructures [9].

As discussed in Sec. II, the relevant electrons occupy the $J = \frac{3}{2}$ and $J = \frac{1}{2}$ multiplets for which we use the following notation:

$$\uparrow = \begin{cases} \left|\frac{3}{2}, +\frac{3}{2}\right\rangle := le\uparrow, \\ \left|\frac{3}{2}, -\frac{1}{2}\right\rangle := he\uparrow, \\ \left|\frac{1}{2}, -\frac{1}{2}\right\rangle := so\uparrow, \end{cases} \qquad \downarrow = \begin{cases} \left|\frac{3}{2}, -\frac{3}{2}\right\rangle := le\downarrow, \\ \left|\frac{3}{2}, +\frac{1}{2}\right\rangle := he\downarrow, \\ \left|\frac{1}{2}, +\frac{1}{2}\right\rangle := so\downarrow. \end{cases} \tag{2}$$

We give these states in terms of $d_{xy}$, $d_{yz}$, and $d_{zx}$ in Supplemental Material S1 [39]. Since we focus on the interaction and splitting of the $\uparrow$ and $\downarrow$ states, we write the Hamiltonian as a block matrix:

$$H = \begin{pmatrix} H_{\uparrow\uparrow} & H_{\uparrow\downarrow} \\ H_{\downarrow\uparrow} & H_{\downarrow\downarrow} \end{pmatrix}. \tag{3}$$

The diagonal blocks $H_{\uparrow\uparrow}$ and $H_{\downarrow\downarrow}$ give the spin degenerate bands. The interaction between the $\uparrow$ and the $\downarrow$ states is governed by the off-diagonal blocks $H_{\uparrow\downarrow}$ and $H_{\downarrow\uparrow}$. In Secs. IV and V we cast the LK Hamiltonian and the $\gamma$ model in a $|J,m_j\rangle$ basis to allow a direct comparison of the coupling term $H_{\uparrow\downarrow}$.

## IV. DETERMINATION OF $H_{\uparrow\downarrow}$ IN THE LK FORMALISM

As discussed in Sec. II, near $\Gamma$ the $t_{2g}$ bands of cubic $SrTiO_3$ neglecting SO are described by the $\mathbf{k}\cdot\mathbf{p}$

Hamiltonian [33,36,37,40],

$$H_{\text{cubic}}\begin{pmatrix} d_{yz} \\ d_{zx} \\ d_{xy} \end{pmatrix} = \begin{pmatrix} Lk_x^2 + M\left(k_y^2 + k_z^2\right) & Nk_xk_y & Nk_xk_z \\ Nk_xk_y & Lk_y^2 + M\left(k_x^2 + k_z^2\right) & Nk_yk_z \\ Nk_xk_z & Nk_yk_z & Lk_z^2 + M\left(k_x^2 + k_y^2\right) \end{pmatrix}\begin{pmatrix} d_{yz} \\ d_{zx} \\ d_{xy} \end{pmatrix}. \quad (4)$$

For convenience, throughout this paper we write the wave vector $k$ in dimensionless units, i.e., multiplied by the lattice vector $a = 3.905$ Å$^{-1}$. These bands are all twofold degenerate when spin is considered. The effective mass parameters $L = 40.03$ meV, $M = 638$ meV, and $N = 105.9$ meV, and the SO splitting $\Delta_{\text{SO}} = 28.5$ meV have been determined for $SrTiO_3$ in Ref. [33] by comparison to density functional theory (DFT) calculations.

Figure 2(a) shows the $t_{2g}$ ($d_{xy}$, $d_{yz}$, and $d_{zx}$) bulk bands according to this model in comparison with the DFT calculations.

We note that along the $(0,0,k_z)$ direction, all off-diagonal terms of Eq. (4) vanish, leaving the parabolic dispersion given by the diagonal elements. The $d_{yz}$ and $d_{zx}$ are degenerate with light effective mass ($\propto 1/M$) while the $d_{xy}$ has a heavy effective mass ($\propto 1/L$). Moreover, if $N$ would be zero, all off-diagonal terms would vanish also along the in-plane directions, with an opposite character of the effective masses. For instance, the $d_{xy}$ band which is heavy along the $\Gamma$-$Z$ direction $(0,0,k)$ would have a light mass ($\propto 1/M$) in the $\Gamma$-$M$ direction $(k,k,0)$. We note, however, that, along $\Gamma$-$M$, the three bands are nondegenerate [33,41], which requires $N \neq 0$, although recent experiments suggest $N = 0$ [42]. This fact is important for the evaluation of the Rashba splitting, as we show below.

The SO interaction is added to the Hamiltonian. In the $|J,m_j\rangle$ basis the additional term is diagonal,

$$H_{\text{SO}} = \frac{\Delta_{\text{SO}}}{3}\text{diag}[-1,-1,-1,-1,2,2]. \quad (5)$$

The total Hamiltonian is given by

$$H^{\text{LK}} = H_{\text{cubic}} + H_{\text{SO}}. \quad (6)$$

Since our main aim is to establish the appropriate model to describe the STO spin-orbit coupled bands, in this study we neglect the small tetragonal distortion occurring below $T = 110$ K [43] and refer to Ref. [33] for more details.

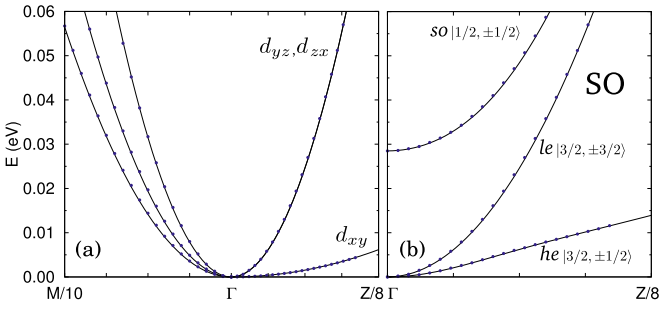


FIG. 2. $\mathbf{k}\cdot\mathbf{p}$ model (lines) and DFT calculations [33] (dots) of the band structure of bulk $SrTiO_3$ around $\Gamma$. Left panel: No SO, Eq. (4). The nondegenerate bands along $\Gamma$-$M$ require $N \neq 0$ (see text). Right panel: With SO, Eq. (6).

The bands calculated according to Eq. (6) with $\Delta_{\text{SO}} = 28.5$ meV are shown in Fig. 2(b) in comparison to DFT calculations. In our calculations we shift the energy origin by $\Delta_{\text{SO}}/3$ so that the band edge of the $J = \frac{3}{2}$ multiplet remains at $E = 0$. The SO interaction lifts the degeneracy of the $d_{yz}$ and $d_{zx}$ bands. One of them is lifted up in energy by $\Delta_{\text{SO}}$ becoming the split-off $so|\frac{1}{2},\pm\frac{1}{2}\rangle$ while the other becomes the pure $le|\frac{3}{2},\pm\frac{3}{2}\rangle$ keeping the same light effective mass ($\propto 1/M$). The $so$ band is coupled to the $he|\frac{3}{2},\pm\frac{1}{2}\rangle$ band and the increased energy separation reduces the $d_{xy}$ effective mass $m_{xy} = 6.2m_e$ to $m_{he} = 1.2m_e$. Most of the literature about the Rashba splitting still describes the results in terms of the $d$ states, which is, strictly speaking, not correct in the presence of SO coupling. Nevertheless, qualitatively, the feature of two bands, one with very heavy mass and another with lighter mass in the quantization direction and opposite behavior in the in-plane direction, leading to subband crossing, is common to the two descriptions. The effect of a quantizing potential is further described in Sec. VII.

When written in the $|J,m_j\rangle$ basis, the Hamiltonian is of the form of Eq. (3). The explicit form of $H_{\uparrow\uparrow}$ and $H_{\downarrow\downarrow}$ is given in Sec. S2 of the Supplemental Material [39]. Here, we focus on the off-diagonal blocks that couple the $\uparrow$ and $\downarrow$ states,

$$H^{\text{LK}}_{\uparrow\downarrow}\begin{pmatrix} le\downarrow \\ he\downarrow \\ so\downarrow \end{pmatrix} = Nk_z\begin{pmatrix} 0 & \frac{-i}{\sqrt{3}}k_- & \frac{1}{\sqrt{6}}k_- \\ \frac{i}{\sqrt{3}}k_- & 0 & \frac{1}{\sqrt{2}}k_+ \\ \frac{1}{\sqrt{6}}k_- & \frac{1}{\sqrt{2}}k_+ & 0 \end{pmatrix}\begin{pmatrix} le\downarrow \\ he\downarrow \\ so\downarrow \end{pmatrix}, \quad (7)$$

with $k_\pm = k_x \pm ik_y$.

This matrix is nonzero also in bulk $SrTiO_3$ but does not lead to any spin splitting there, as it should not by spatial and time inversion symmetry. In heterostructures, however, $k_z$ is an operator and $H_{\uparrow\downarrow}$ splits $\uparrow$ and $\downarrow$ states in the absence of spatial inversion symmetry, resulting in a Rashba spin splitting proportional to $N$.

## V. $\gamma$ MODEL IN THE $|J,m_j\rangle$ BASIS

In Refs. [22,24] where $N$ is assumed to be zero, the phenomenological term $H^\gamma$ [Eq. (1)] is added to a tight-binding Hamiltonian to account for the extra hopping terms between the $d_{xy}$ and $d_{yz}$,$d_{zx}$ states due to deformation of the atomic orbitals by an internal electric field at the interface [22–24]. We study the effect of this type of Rashba spin splitting within the envelope function method, defining the $\gamma$ model as $H^{\text{LK}}(N = 0) + H^\gamma$.

Here, we write $H^\gamma$ [Eq. (1)] in the $|J,m_j\rangle$ basis to allow a direct comparison with $H^{\text{LK}}_{\uparrow\downarrow}$. Using the approximation

$\sin(k_x) \approx k_x$, we find

$$H^{\gamma}_{\uparrow\downarrow}\begin{pmatrix} le\downarrow \\ he\downarrow \\ so\downarrow \end{pmatrix} = 2i\gamma \begin{pmatrix} 0 & -\frac{i}{\sqrt{3}}k_- & \frac{1}{\sqrt{6}}k_- \\ -\frac{i}{\sqrt{3}}k_- & -\frac{2i}{3}k_+ & -\frac{1}{3\sqrt{2}}k_+ \\ -\frac{1}{\sqrt{6}}k_- & \frac{1}{3\sqrt{2}}k_+ & \frac{2i}{3}k_+ \end{pmatrix} \begin{pmatrix} le\downarrow \\ he\downarrow \\ so\downarrow \end{pmatrix}. \tag{8}$$

## VI. COMPARISONS OF $H_{\uparrow\downarrow}$ IN THE $\gamma$ AND LK MODEL

In this section we compare the effect of the coupling matrix $H_{\uparrow\downarrow}$ in the $\gamma$ and LK models on the spin splitting in an asymmetric confining potential. Despite a similar structure, the two coupling matrices Eqs. (7) and (8) present important differences. First, $H^{\mathrm{LK}}_{\uparrow\downarrow}$ is proportional to $k_z$, which in a confining potential becomes an operator, whereas $H^{\gamma}_{\uparrow\downarrow}$ is proportional to the scalar $\gamma$. Second, each imaginary component in the elements of one matrix is real in the other and vice versa. Third, and most important, not all diagonal elements of $H^{\gamma}_{\uparrow\downarrow}$ are zero, giving a direct coupling between $he\uparrow$ and $he\downarrow$ and between $so\uparrow$ and $so\downarrow$. It is this feature that eventually leads to the much larger spin splitting of the lowest subband that we describe in the next section.

Close to $\Gamma$, the $\gamma$ model gives linear $k$ splitting for $he$ subbands, and $k^3$ splitting for $le$ subbands. For the LK model, due to the zero valued diagonal elements, it is the mixed $so$,$he$ character of the lowest bulk band that gives rise to a linear splitting. In fact, the $he$ and $so$ states are coupled by terms in $k_z k_\pm$ and $k_z^2$ that couple states of different space parities. When the parity of the states is broken by the electric field, the coupling occurs also with the same subband and results in a linear spin-orbit splitting. The pure $le$ bulk band, instead, has a $k^3$ splitting due to a two-step coupling.

Due to the different coupling mechanism in the two models, a single value of $\gamma$ can reproduce only either the linear or the cubic splitting for a given electric field. We found that fitting $\gamma$ to the linear splitting gives a much better overall agreement (whereas fitting of the cubic splitting largely overestimates the splittings). Therefore we identify, for every value of the electric field, a parameter $\gamma_{\mathrm{fit}}$ that gives the same linear spin splitting of the lowest subband in both models. As shown in detail in Sec. S4 of the Supplemental Material [39], $\gamma_{\mathrm{fit}}$ grows with electric field. This finding is in agreement with the observation of increased SO coupling with carrier concentration discussed in Ref. [5].

## VII. NUMERICAL EVALUATION: COMPARISON OF THE RASHBA SPIN SPLITTING IN THE LK MODEL AND THE $\gamma$ MODEL

Here, we compare the Rashba spin splitting of the LK and the $\gamma$ model. We consider a triangular confining potential $V(z) = Fz$ resulting from a constant electric field with electric field strength $F$. We find the quantized subbands by solving the eigenvalue problem by finite differences as described in Ref. [33] and in Sec. S3 of the Supplemental Material [39]. Self-consistent calculations of the potential would lead to a bending at high energies with negligible effects on the lowest subbands, except in the situation where the Fermi energy comes close to the upper edge of the confining potential [44],

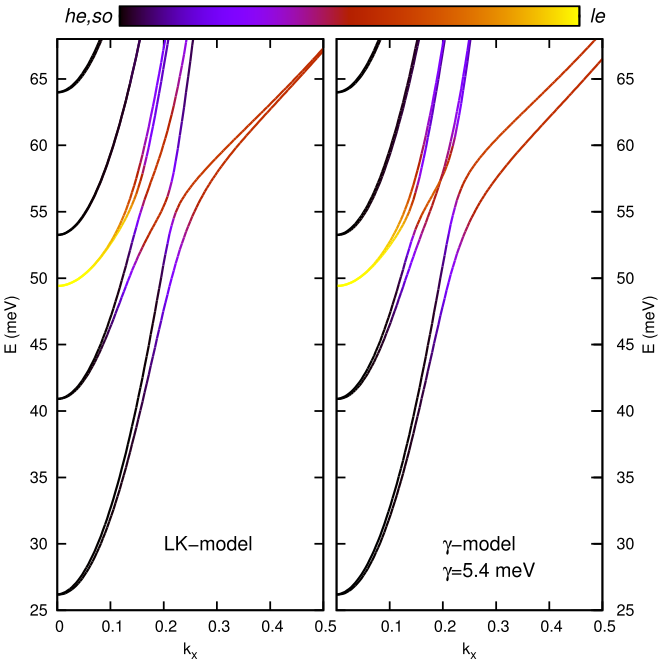


FIG. 3. In-plane dispersion in a triangular well with slope $F = 1.0$ meV/Å according to the LK Hamiltonian (left panel) and the $\gamma$ model with $\gamma = 5.4$ meV (right panel). The color indicates the $he$, $so$, or $le$ character of the subbands.

where it could lead to electronic instabilities [45]. For simplicity, we neglect these effects here.

A triangular potential has the advantage that $\gamma$ depends only on the electric field strength and not on the spatial coordinate $z$. Our method is based on a $\mathbf{k}\cdot\mathbf{p}$ description of the bulk bands around $\Gamma$ which becomes less accurate for large confinement energies, limiting the electric field strength to $F \sim 1.0$ meV/Å.

We point out that the envelope function method gives all the quantized subbands. For example, it is possible to have more than one subband with the same character at $\Gamma$, as can be seen in Fig. 3. In other studies instead [15,24] only one $he$, one $le$, and one $so$ subband are calculated and the quantization energy is chosen as a parameter $\Delta_I$.

In Fig. 3 we show the subbands calculated within the two models for $F = 1.0$ meV/Å, where two $he$ subbands are lower than the first $le$ subband, as indicated by the color coding. One can see that the $le$ subband, which has a heavy mass in the $xy$ plane, anticrosses the two $he$ subbands at $E \sim 55$ meV. At this anticrossing, which has also been identified as a Lifshitz point [3,15,46], the Rashba spin splitting is largest in both models. For this electric field strength, at $\Gamma$, we find that the lowest $he$ subband is $\approx$22 meV below the lowest $le$ subband, to be compared to $\sim$ 60–90 meV [46–49] and much larger splittings of $>$200 meV [16,24,50,51] found in other work.

Up to the anticrossing both models give very similar subbands, as guaranteed by the choice of $\gamma_{\mathrm{fit}}$. At larger energies, the subbands start to mix, producing clear differences between the two models. The most important difference is that the Rashba spin splitting of the lowest subband after the anticrossing decreases in the LK model, whereas it remains large in the $\gamma$ model. The splitting of the second band is also

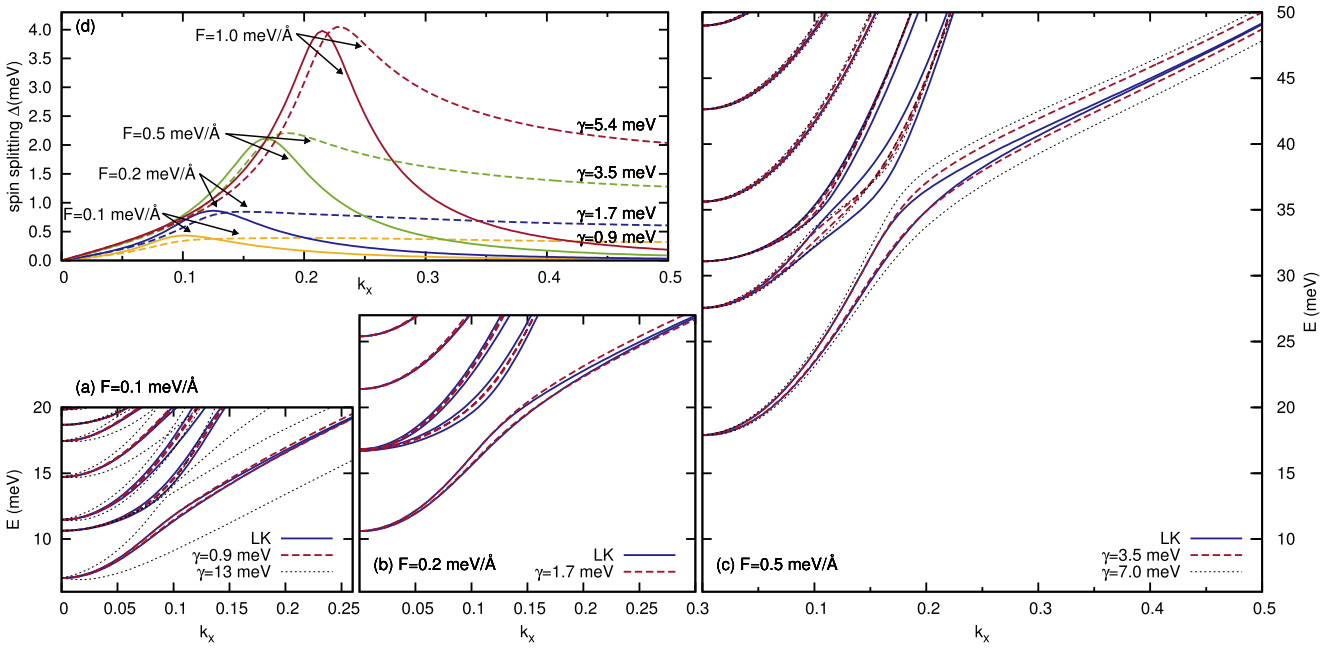


FIG. 4. Subbands for (a) $F = 0.1$ meV/Å, (b) 0.2 meV/Å, (c) 0.5 meV/Å, and (d) spin splitting $\Delta$ of the lowest subband for four values of $F$. The solid line is the LK model, and the dashed line the $\gamma$ model with $\gamma_{\text{fit}}$. The dotted lines in (a) and (c) correspond to larger values of $\gamma$. In (d) we show the spin splitting of the lowest subband. The spin splitting is very sensitive to the choice of the parameter $\gamma$. In (a) we show the subbands for $\gamma = 13$ meV, which is the value that gives the same cubic splitting of the $le$ (see Supplemental Material S4 [39]) and in (c) we show the effect of doubling $\gamma$.

quite different in the two models, with a crossing in the $\gamma$ model. Since the experimental evidence of Rashba spin splitting comes mainly from transport measurements [4,10–14,14], such a different dispersion at large $k$ is highly significant for the interpretation of experimental data. SdH experiments should be able to distinguish between the resulting different shapes of the Fermi surface, if the Fermi energy could be changed continuously by means of external gating. Moreover, the different composition of the subband eigenvectors affects the spin orientation and would lead to different spin textures, as described in Sec. 6.6 of Ref. [9].

In Fig. 4 we compare the two models for three different values of the electric field $F$. As $F$ increases, the potential well becomes steeper, and the subbands move upwards in energy to an extent that depends on their respective effective masses. Due to the nonparabolicity of the SO coupled bulk bands [33], the order of the bands changes from $he_1$, $le_1$, $he_2$ for $F = 0.1$ and 0.2 meV/Å to $he_1$, $he_2$, $le_1$ for $F = 0.5$ meV/Å as for $F = 1.0$ meV/Å shown in Fig. 3. Other than this difference, the main features remain unchanged: The two models agree well for energies well under the anticrossing, but the splitting is fundamentally different at higher energies. The LK model gives a splitting at every anticrossing. The size of the splitting grows with the electric field because the anticrossing occurs at larger and larger values of the momentum, which determines the amount of coupling. Moreover, the splitting decreases away from the anticrossing. The $\gamma$ model, on the other hand, gives splitting only at the lowest anticrossing and the splitting remains large away from the anticrossing, due to the direct coupling of $he_\uparrow$ and $he_\downarrow$ described in Sec. VI. We emphasize again that the spin splitting is in the range of resolution of SdH experiments [35]. For instance, for $F = 0.5$ meV/Å and a Fermi energy of 35 meV, one should be able to resolve the spin splitting of at least two of the three subbands crossing the Fermi energy.

## VIII. SUMMARY AND PERSPECTIVES

In summary, we have examined the Rashba spin splitting in STO-based heterostructures. We have compared in detail the results of the Luttinger-Kohn effective mass model of the $t_{2g}$ edge with a phenomenological model of the spin splitting inspired by the two-band model of Rashba. The latter has the advantage of being simple to implement but has a weaker physical basis than the $\mathbf{k} \cdot \mathbf{p}$ model, for which spin splitting in asymmetric confining potentials results naturally, without the addition of phenomenological parameters. We have pointed out that a discussion of the Rashba spin splitting in asymmetric potentials requires one to go over from a description in terms of the $d$ orbitals to the SO coupled $t_{2g}$ states, a basis which is intrinsic to the LK model. We have shown that the LK model predicts that spin splitting arises at the avoided crossing of the SO coupled subbands, and decreases away from them. The $\gamma$ model has a very different, possibly unphysical, behavior in this range. Establishing the correct model to describe the Rashba spin splitting in oxide materials is important for a whole class of new 2D systems [18,19,21] in correlated materials.

## ACKNOWLEDGMENTS

This work is part of the research program of the Stichting voor Fundamenteel Onderzoek der Materie (FOM), which is financially supported by the Nederlandse Organisatie voor Wetenschappelijk Onderzoek (NWO). A.F. and A.M. thank M. Salluzzo and A.F. thanks C. Noguera for fruitful discussions.

[1] A. Ohtomo and H. Hwang, Nature (London) **427**, 423 (2004).
[2] A. D. Caviglia, S. Gariglio, N. Reyren, D. Jaccard, T. Schneider, M. Gabay, S. Thiel, G. Hammerl, J. Mannhart, and J.-M. Triscone, Nature (London) **456**, 624 (2008).
[3] J. Ruhman, A. Joshua, S. Ilani, and E. Altman, Phys. Rev. B **90**, 125123 (2014).
[4] A. D. Caviglia, M. Gabay, S. Gariglio, N. Reyren, C. Cancellieri, and J.-M. Triscone, Phys. Rev. Lett. **104**, 126803 (2010).
[5] D. Stornaiuolo, S. Gariglio, A. Fête, M. Gabay, D. Li, D. Massarotti, and J.-M. Triscone, Phys. Rev. B **90**, 235426 (2014).
[6] J. Biscaras, N. Bergeal, S. Hurand, C. Feuillet-Palma, A. Rastogi, R. C. Budhani, M. Grilli, S. Caprara, and J. Lesueur, Nat. Mater. **12**, 542 (2013).
[7] D. Bucheli, M. Grilli, F. Peronaci, G. Seibold, and S. Caprara, Phys. Rev. B **89**, 195448 (2014).
[8] J. A. Sulpizio, S. Ilani, P. Irvin, and J. Levy, Annu. Rev. Mater. Res. **44**, 117 (2014).
[9] R. Winkler, *Spin Orbit Coupling Effects in Two-Dimensional Electron and Hole Systems* (Springer, New York, 2003).
[10] H. Nakamura, T. Koga, and T. Kimura, Phys. Rev. Lett. **108**, 206601 (2012).
[11] A. Fête, S. Gariglio, A. D. Caviglia, J.-M. Triscone, and M. Gabay, Phys. Rev. B **86**, 201105 (2012).
[12] A. Fête, S. Gariglio, C. Berthod, D. Li, D. Stornaiuolo, M. Gabay, and J.-M. Triscone, New J. Phys. **16**, 112002 (2014).
[13] M. Ben Shalom, M. Sachs, D. Rakhmilevitch, A. Palevski, and Y. Dagan, Phys. Rev. Lett. **104**, 126802 (2010).
[14] H. Liang, L. Cheng, L. Wei, Z. Luo, G. Yu, C. Zeng, and Z. Zhang, Phys. Rev. B **92**, 075309 (2015).
[15] M. Diez, A. M. R. V. L. Monteiro, G. Mattoni, E. Cobanera, T. Hyart, E. Mulazimoglu, N. Bovenzi, C. W. J. Beenakker, and A. D. Caviglia, Phys. Rev. Lett. **115**, 016803 (2015).
[16] P. D. C. King, S. McKeown Walker, A. Tamai, A. de la Torre, T. Eknapakul, P. Buaphet, S.-K. Mo, W. Meevasana, M. S. Bahramy, and F. Baumberger, Nat. Commun. **5**, 3414 (2014).
[17] M. Kim, C. Bell, Y. Kozuka, M. Kurita, Y. Hikita, and H. Y. Hwang, Phys. Rev. Lett. **107**, 106801 (2011).
[18] Y. Xu, I. Miotkowski, C. Liu, J. Tian, H. Nam, N. Alidoust, J. Hu, C.-K. Shih, M. Zahid Hasan, and Y. P. Chen, Nat. Phys. **10**, 956 (2014).
[19] W. Witczak-Krempa, G. Chen, Y. B. Kim, and L. Balents, Annu. Rev. Condens. Matter Phys. **5**, 57 (2014).
[20] E. Lake, C. Webb, D. A. Pesin, and O. A. Starykh, Phys. Rev. B **93**, 214516 (2016).
[21] S. Banerjee, J. Rowland, O. Erten, and M. Randeria, Phys. Rev. X **4**, 031045 (2014).
[22] G. Khalsa, B. Lee, and A. H. MacDonald, Phys. Rev. B **88**, 041302 (2013).
[23] L. Petersen and P. Hedegård, Surf. Sci. **459**, 49 (2000).
[24] Z. Zhong, A. Tóth, and K. Held, Phys. Rev. B **87**, 161102 (2013).
[25] Y. Kim, R. M. Lutchyn, and C. Nayak, Phys. Rev. B **87**, 245121 (2013).
[26] J. Zhou, W. Y. Shan, and D. Xiao, Phys. Rev. B **91**, 241302 (2015).
[27] J. M. Luttinger and W. Kohn, Phys. Rev. **97**, 869 (1955).
[28] G. Goldoni and A. Fasolino, Phys. Rev. Lett. **69**, 2567 (1992).
[29] E. A. de Andrada e Silva, G. C. La Rocca, and F. Bassani, Phys. Rev. B **50**, 8523 (1994).
[30] Th. Schäpers, G. Engels, J. Lange, Th. Klocke, M. Hollfelder, and H. Lüth, J. Appl. Phys. **83**, 4324 (1998).
[31] G. Engels, J. Lange, Th. Schäpers, and H. Lüth, Phys. Rev. B **55**, R1958 (1997).
[32] T. Koga, J. Nitta, T. Akazaki, and H. Takayanagi, Phys. Rev. Lett. **89**, 046801 (2002).
[33] L. W. van Heeringen, G. A. de Wijs, A. McCollam, J. C. Maan, and A. Fasolino, Phys. Rev. B **88**, 205140 (2013).
[34] J. Mannhart and D. Schlom, Science **327**, 1607 (2010).
[35] A. McCollam, S. Wenderich, M. K. Kruize, V. K. Guduru, H. J. A. Molegraaf, M. Huijben, G. Koster, D. H. A. Blank, G. Rijnders, A. Brinkman, H. Hilgenkamp, U. Zeitler, and J. C. Maan, APL Mater. **2**, 022102 (2014).
[36] M. S. Dresselhaus, G. Dresselhaus, and A. Jorio, *Group Theory: Application to the Physics of Condensed Matter* (Springer, Berlin, 2008).
[37] L. van Heeringen, Master's thesis, Radboud University, 2012.
[38] Y. A. Bychkov and E. I. Rashba, JETP Lett. **39**, 78 (1984).
[39] See Supplemental Material at http://link.aps.org/supplemental/10.1103/PhysRevB.95.155134 for explicit expressions of the basis states and of $H_{\uparrow\uparrow}$ and $H_{\downarrow\downarrow}$, envelope function method, and choice of the value of $\gamma$.
[40] R. Bistritzer, G. Khalsa, and A. H. MacDonald, Phys. Rev. B **83**, 115114 (2011).
[41] A. Janotti, D. Steiauf, and C. G. Van de Walle, Phys. Rev. B **84**, 201304(R) (2011).
[42] S. J. Allen, B. Jalan, S. B. Lee, D. G. Ouellette, G. Khalsa, J. Jaroszynski, S. Stemmer, and A. H. MacDonald, Phys. Rev. B **88**, 045114 (2013).
[43] L. F. Mattheiss, Phys. Rev. B **6**, 4740 (1972).
[44] J. Biscaras, S. Hurand, C. Feuillet-Palma, A. Rastogi, R. C. Budhani, N. Reyren, E. Lesne, J. Lesueur, and N. Bergeal, Sci. Rep. **4**, 6788 (2014).
[45] N. Scopigno, D. Bucheli, S. Caprara, J. Biscaras, N. Bergeal, J. Lesueur, and M. Grilli, Phys. Rev. Lett. **116**, 026804 (2016).
[46] A. Joshua, S. Pecker, J. Ruhman, E. Altman, and S. Ilani, Nat. Commun. **3**, 1129 (2012).
[47] A. F. Santander-Syro, O. Copie, T. Kondo, F. Fortuna, S. Pailhès, R. Weht, X. G. Qiu, F. Bertran, A. Nicolaou, A. Taleb-Ibrahimi *et al.*, Nature (London) **469**, 189 (2011).
[48] M. Salluzzo, J. C. Cezar, N. B. Brookes, V. Bisogni, G. M. De Luca, C. Richter, S. Thiel, J. Mannhart, M. Huijben, A. Brinkman *et al.*, Phys. Rev. Lett. **102**, 166804 (2009).
[49] C. Cancellieri, M. L. Reinle-Schmitt, M. Kobayashi, V. N. Strocov, P. R. Willmott, D. Fontaine, Ph. Ghosez, A. Filippetti, P. Delugas, and V. Fiorentini, Phys. Rev. B **89**, 121412(R) (2014).
[50] N. C. Plumb, M. Salluzzo, E. Razzoli, M. Månsson, M. Falub, J. Krempasky, C. E. Matt, J. Chang, M. Schulte, J. Braun *et al.*, Phys. Rev. Lett. **113**, 086801 (2014).
[51] P. Delugas, A. Filippetti, V. Fiorentini, D. I. Bilc, D. Fontaine, and P. Ghosez, Phys. Rev. Lett. **106**, 166807 (2011).